2492 *Inorg. Chem.* **2010**, *49*, 2492–2495
DOI: 10.1021/ic9024876

Inorganic Chemistry
Article

Antiferromagnetic Interaction between *A*′-Site Mn Spins in *A*-Site-Ordered Perovskite $YMn_3Al_4O_{12}$

Takenori Tohyama,*,† Takashi Saito,† Masaichiro Mizumaki,‡ Akane Agui,§ and Yuichi Shimakawa†

†*Institute for Chemical Research, Kyoto University, Uji, Kyoto 611-0011, Japan,* ‡*Japan Synchrotron Radiation Research Institute, Spring-8, 1-1-1 Kouto, Sayo-cho, Sayo-gun, Hyogo 679-5198, Japan, and* §*Synchrotron Radiation Research Center, Japan Atomic Energy Agency, Spring-8, 1-1-1 Kouto, Sayo-cho, Sayo-gun, Hyogo 679-5148, Japan*

Received December 15, 2009

The *A*-site-ordered perovskite $YMn_3Al_4O_{12}$ was prepared by high-pressure synthesis. Structural analysis with synchrotron powder X-ray diffraction data and the Mn *L*-edges X-ray absorption spectrum revealed that the compound has a chemical composition $Y^{3+}Mn^{3+}{}_3Al^{3+}{}_4O^{2-}{}_{12}$ with magnetic Mn^{3+} at the *A*′ site and non-magnetic Al^{3+} at the *B* site. An antiferromagnetic interaction between the *A*′-site Mn^{3+} spins is induced by the nearest neighboring Mn−Mn direct exchange interaction and causes an antiferromagnetic transition at 34.3 K.

Introduction

Much attention has been paid to *A*-site-ordered perovskites with a chemical composition of $AA'_3B_4O_{12}$ because they show intriguing physical properties,[1] some of which will be useful for future applications. For example, $ACu_3Mn_4O_{12}$ (A = Ca, La, and Bi) show colossal magnetoresistance at low magnetic fields,[2−4] and $CaCu_3Ti_4O_{12}$ shows giant permittivity at temperatures around room temperature.[5] The *A* and *A*′ ions in this structure are located at the *A* site of a simple ABO_3 perovskite, and they are ordered as shown in Figure 1. The *A*′ site is usually occupied by Jahn−Teller active ions such as Cu^{2+} and Mn^{3+}. These ions at the originally 12-fold-coordinated position are stabilized there because the BO_6 octahedra are significantly tilted, resulting in $A'O_4$ square-planar coordination.

When an *A*-site ordered perovskite contains Cu at the *A*′ site, those Cu ions play an important role in giving rise to a wide variety of physical properties. In magnetoresistive $ACu_3Mn_4O_{12}$ (A = Ca, La, and Bi), the *A*′-site Cu spins couple with the *B*-site Mn spins antiferromagnetically, leading to ferrimagnetism with transition temperatures above room temperature.[2−4] Electronic behavior of $ACu_3Ru_4O_{12}$ is metallic with heavy effective mass without f-electrons.[6−8] A temperature-induced intersite charge transfer between the *A*′-site Cu and the *B*-site Fe was recently found in $LaCu_3Fe_4O_{12}$ ($Cu^{2+} + Fe^{+3.75} \rightarrow Cu^{3+} + Fe^{3+}$).[9] When the *B* site contains non-magnetic ions, on the other hand, we can observe *A*′-*A*′ magnetic interaction. The *A*′-site Cu−Cu interaction in $CaCu_3B_4O_{12}$ (B = Ge and Sn) is ferromagnetic because of the direct exchange interaction between the nearest neighboring Cu spin, while that in $CaCu_3Ti_4O_{12}$ is antiferromagnetic primarily because of the Cu−O−Ti−O−Cu superexchange interaction.[10−12]

Since there has been no reports of a compound with *A*′-site Mn ions and *B*-site non-magnetic ions in contrast to the *A*′-site Cu containing compounds, we synthesized $YMn_3Al_4O_{12}$, which has Mn ions at the *A*′ site and non-magnetic Al^{3+} ions at the *B* site. Here we report the magnetic properties of the *A*′-site Mn spins and discuss the *A*′-*A*′ magnetic interaction.

Experimental Section

$YMn_3Al_4O_{12}$ was synthesized under high-pressure and high temperature. Powdered Y_2O_3, Mn_2O_3, and Al_2O_3 were

*To whom correspondence should be addressed. E-mail: tohyama@msk.kuicr.kyoto-u.ac.jp. Phone: +81-774-38-3115. Fax: +81-774-38-3118.

(1) Shimakawa, Y. *Inorg. Chem.* **2008**, *47*, 8562.
(2) Zeng, Z.; Greenblatt, M.; Subramanian, M. A.; Croft, M. *Phys. Rev. Lett.* **1999**, *82*, 3164.
(3) Alonso, J. A.; Sanchez-Benitez, J.; Andres, A. De.; Martinez-Lope, M. J.; Casais, M. T.; Martinez, J. L. *Appl. Phys. Lett.* **2003**, *83*, 2623.
(4) Takata, K.; Yamada, I.; Azuma, M; Takano, M.; Shimakawa, Y. *Phys. Rev. B* **2007**, *76*, 024429.
(5) Ramirez, A. P.; Subramanian, M. A.; Gardel, M.; Blumberg, G.; Li, D.; Vogt, T.; Shapiro, S. M. *Solid State Commun.* **2000**, *115*, 217.
(6) Kobayashi, W.; Terasaki, I.; Takeya, J.; Tsukada, I.; Ando, Y. *J. Phys. Soc. Jpn.* **2004**, *73*, 2373–2376.
(7) Ramirez, A. P.; Lawes, G.; Li, D.; Subramanian, M. A. *Solid State Commun.* **2004**, *131*, 251–255.
(8) Tanaka, S.; Shimazui, N.; Takatsu, H.; Yonezawa, S.; Maeno, Y. *J. Phys. Soc. Jpn.* **2009**, *78*, 024706.
(9) Long, Y. W.; Hayashi, N.; Saito, T.; Azuma, M.; Muranaka, S.; Shimakawa, Y. *Nature* **2009**, *458*, 60.
(10) Shiraki, H.; Saito, T.; Yamada, T.; Tsujimoto, M.; Azuma, M.; Kurata, H.; Isoda, S.; Takano, M.; Shimakawa, Y. *Phys. Rev. B* **2007**, *76*, 140403.
(11) Shiraki, H.; Saito, T.; Shimakawa, Y. *Chem. Mater.* **2008**, *20*, 7077.
(12) Shimakawa, Y.; Shiraki, H.; Saito, T. *J. Phys. Soc. Jpn.* **2008**, *77*, 113702.

Published on Web 01/28/2010

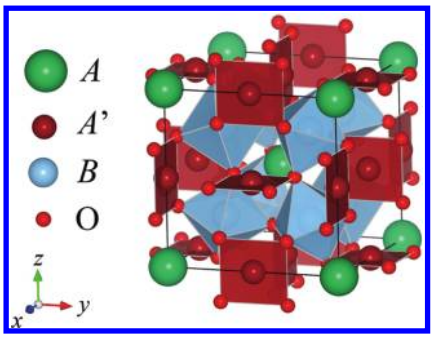

Figure 1. Crystal structure of $AA'_3B_4O_{12}$ perovskite. *A* and *A*′-site ions are ordered at the ratio of 1:3, and *B*-site ions form a heavily tilted octahedral network.

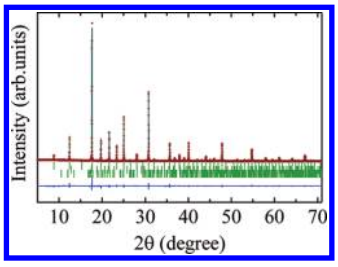

Figure 2. Synchrotron X-ray powder diffraction pattern and the result of Rietveld refinement for $YMn_3Al_4O_{12}$. Vertical marks represent the positions of the Bragg peaks for $YMn_3Al_4O_{12}$ (upper), Al_2O_3 (middle, 1.64 wt %), and $YAlO_3$ (bottom, 0.53 wt %). Also shown at the bottom is the difference between the observed and calculated intensities.

ground in a mortar and packed into a gold capsule. After the mixture was heated to 1173 K and held for 1 h at that temperature and 9 GPa in a multianvil-type high-pressure apparatus, it was slowly cooled to room temperature during the next 5 h.

Synchrotron X-ray powder diffraction pattern of the material thus prepared was collected with a large Debye−Scherrer camera installed at BL02B2 in SPring-8. The sample was packed into a glass capillary 0.1 mm in diameter and was rotated during the measurement. The obtained diffraction data was refined by the Rietveld method using the program RIETAN-2000.[13] At BL27SU in SPring-8 the X-ray absorption spectrum (XAS) of the Mn $L_{2,3}$−edge were also measured.

Magnetic properties of $YMn_3Al_4O_{12}$ were measured using a commercial SQUID magnetometer (MPMS, Quantum Design). The temperature dependence of the magnetic susceptibility was measured in a temperature range of $5\ K \leq T \leq 300\ K$ at a magnetic field of 1 T, and the field dependence of the magnetic moments at 5 K was measured under fields ranging from −10 000 to 10 000 Oe. The heat capacity in a temperature range from 2 to 100 K was measured using a Physical Property Measurement System (PPMS, Quantum Design).

Results and Discussion

Figure 2 shows the synchrotron X-ray diffraction pattern of $YMn_3Al_4O_{12}$ and the results of the Rietveld fitting. Although peaks due to small amounts of impurities (1.64% Al_2O_3 and 0.53% $YAlO_3$) are evident in the diffraction pattern, the main peaks are well reproduced with a cubic $Im\bar{3}$ $AA'_3B_4O_{12}$ perovskite model. In the initial refinement, some anomaly in the diffraction intensities suggested a cation substitution. Incorporation of Mn ions into the *B* site was thus included in the final refinement (4.76% of the *B* sites). No anomaly was seen in the oxygen occupation. The structural parameters obtained from the analysis are listed in Table 1. Selected bond-lengths and angles are also listed in Table 2 along with the bond valence sum (BVS)[14] values calculated from the obtained bond lengths. Four of the twelve Mn−O bond lengths were quite short compared to the other eight bonds, which confirms that the Mn ions are coordinated by four O ions making the MnO_4 square units at the *A*′ site. The BVS values for the *A*-site Y, *A*′-site Mn, and *B*-site Al were respectively +2.92, +3.02, and +2.80, strongly suggesting that each cation has oxidation state of +3. Consequently, the compound should be represented as $Y^{3+}Mn^{3+}{}_3Al^{3+}{}_4O^{2-}{}_{12}$.

Table 1. Refined Structural Parameters Obtained for $YMn_3Al_4O_{12}$ by Rietveld Analysis

atom	site	*x*	*y*	*z*	U_{iso}(Å^2)
Y	2*a*	0.0	0.0	0.0	0.0019(1)
Mn	6*b*	0.0	0.5	0.5	0.0041(5)
Al	8*c*	0.25	0.25	0.25	0.0025(5)
O	24*g*	0.1809(5)	0.3034(7)	0.0	0.0067(5)
lattice constant (Å)					7.1796(2)
R_{WP}(%)					4.89
R_P(%)					3.43

Table 2. Selected Bond Lengths, Bond Angles, and Bond Valence Sum Values for Constituent Cations[a]

Bond Lengths	
Mn−O (Å)	1.918(0) × 4
	2.690(4) × 4
	3.161(4) × 4
Mn−Mn (Å)	3.589(8)
Bond Angles	
Mn−O−Mn (deg)	101.00(4)
Al−O−Al (deg)	141.48(8)
Bond Valence Sums	
(Y)	2.92
(Mn)	3.02
(Al)	2.80

[a] Note that four of the twelve Mn−O bond distances are extremely short relative to the others, suggesting that the Mn ion at the *A*′ site is coordinated by four O^{2-} ions.

The X-ray absorption spectrum (XAS) of the Mn $L_{2,3}$-edges for $YMn_3Al_4O_{12}$ is shown in Figure 3, together with the previously reported XAS spectra for the Mn $L_{2,3}$-edges of $LaMn_3Ti_4O_{12}$ and $LaMn_3Cr_4O_{12}$.[15] The spectral shape of $YMn_3Al_4O_{12}$ is quite similar to that of $La^{3+}Mn^{3+}{}_3Cr^{3+}{}_4O_{12}$ with Mn^{3+} at the *A*′ site but is very different from that of $La^{3+}Mn^{1.67+}{}_3Ti^{4+}{}_4O_{12}$, where the ionic state of Mn at the *A*′ site is less than +2. Especially the Mn-*L* absorption edge energies of $YMn_3Al_4O_{12}$ are higher than those of $LaMn_3Ti_4O_{12}$. This chemical shift also confirms that the ionic state of Mn in $YMn_3Al_4O_{12}$ is very close to +3.

Since the results of the structure analysis and the chemical shift in the XAS spectrum clearly indicate that our $YMn_3Al_4O_{12}$ contains magnetic Mn^{3+} at the *A*′ site and non-

(13) Izumi, F.; Ikeda, T. *Mater. Sci. Forum* **2000**, *321*−*324*, 198.

(14) Brown, I. D.; Altermatt, D. *Acta Crystallogr.* **1985**, *B41*, 244.

(15) Long, Y. W.; Saito, T.; Mizumaki, M.; Agui, A.; Shimakawa, Y. *J. Am. Chem. Soc.* **2009**, *131*, 16244.

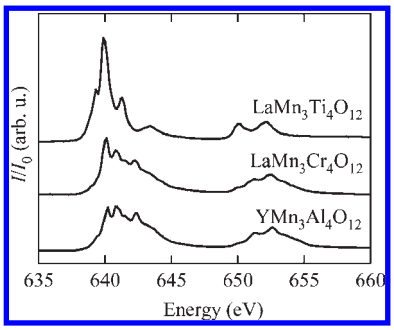

Figure 3. X-ray absorption spectra of Mn $L_{2,3}$-edges of $LaMn_3Ti_4O_{12}$ (upper), $LaMn_3Cr_4O_{12}$ (middle), and $YMn_3Al_4O_{12}$ (bottom).

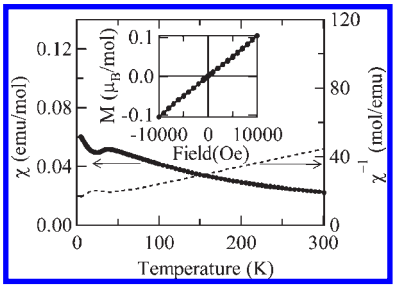

Figure 4. Temperature dependence of the magnetic susceptibility of $YMn_3Al_4O_{12}$ measured in a 1 T external field. The inset shows the field dependence of the magnetic moment measured at 5 K.

magnetic Al^{3+} at the *B* site, it should be interesting to investigate the magnetic interaction between the *A*′-site Mn^{3+} ions. The temperature dependence of the magnetic susceptibility measured in a magnetic field of 1 T is shown for $YMn_3Al_4O_{12}$ in Figure 4 (a χ-*T* graph). The field dependence of the magnetic moment measured at 5 K (an *M*-*H* graph) is shown in the inset. Near 35 K in the χ-*T* graph there is a peak indicating an antiferromagnetic transition. Neither a hysteresis loop nor a large induced magnetic moment was observed in the *M*-*H* measurement. As shown in Figure 5, the heat capacity of this compound also shows a λ-type transition at 34.3 K. Above the transition temperature, the magnetic susceptibility obeys the Curie−Weiss law. Fitting the observed data to a Curie−Weiss formula, $\chi = C/(T - \theta)$, gave a Curie constant of 9.62 emu/mol/K and a Weiss temperature of −129 K. The negative Weiss temperature is consistent with the antiferromagnetic property. The effective magnetic moment obtained from the Curie constant was 5.06 μ_B/Mn, which is close to the 4.90 μ_B expected for a high-spin state of Mn^{3+} ($S = 2$). We can thus conclude from the above measurements that $YMn_3Al_4O_{12}$ is an antiferromagnet with high-spin Mn^{3+} ions at the *A*′ site. The small amount of Mn ions at the *B* site had no significant effect on the measured magnetic susceptibility.

The electronic structure of $YMn_3Al_4O_{12}$ was calculated by full-potential linearized augmented plane wave (FLAPW) first principle calculations with the WIEN-2k code[16] within the generalized gradient approximation exchange-correlation function to investigate the magnetic interaction between the Mn spins in detail. The structural parameters obtained from the above structural refinements were used for these

(16) Blaha, P.; Schwarz, K.; Madsen, G. K. H.; Kvasnicka, D.; Luitz, J. *WIEN2k, an Augmented Plane Wave+Local Orbitals Program for Calculating Crystal Properties*; Vienna University of Technology: Vienna, Austria, 2002.

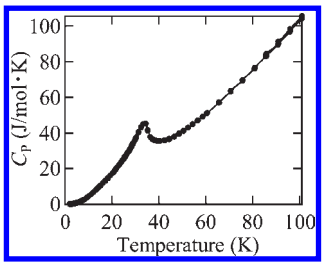

Figure 5. Heat capacity, C_p, of $YMn_3Al_4O_{12}$.

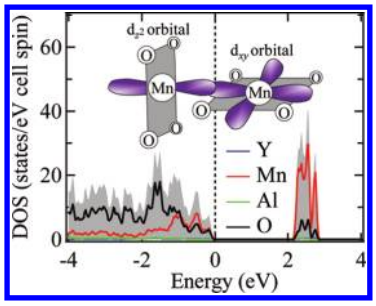

Figure 6. Calculated up-spin density of states (DOS) of $YMn_3Al_4O_{12}$. Because the compound is an antiferromagnet, the down-spin DOS is the same as the up-spin DOS. The partial DOS for each constituent atom is also shown. The inset shows a schematic drawing of orbitals of *A*′-site Mn ions in the MnO_4 square units.

calculations. The FLAPW sphere radii used for Y, Mn, Al, and O were respectively 2.4, 2.0, 1.8, and 1.6 au. Electronic structures for ferromagnetic and antiferromagnetic arrangements of Mn^{3+} spins were calculated with the $Pm\bar{3}$ structural model. The calculation confirmed that the antiferromagnetic state is 207.5 meV more stable than the ferromagnetic one, which is consistent with the experimental results of the magnetic measurements. Figure 6 shows the calculated density of states of the antiferromagnetic $YMn_3Al_4O_{12}$. The obtained energy gap was about 2 eV, which is consistent with the insulating behavior of the brown-colored sample. Note that the bands near the Fermi energy are due largely to the Mn-3d and O-2p orbitals and that contributions to these bands from Y or Al orbitals are negligible. This implies that the Al orbitals do not hybridize with Mn-3d or O-2p orbitals near the Fermi energy and that they do not contribute to the magnetic interactions between the Mn^{3+} spins. This differs markedly from the antiferromagnetism in $CaCu_3Ti_4O_{12}$, where the orbital hybridization of the non-magnetic Ti^{4+} ions at the *B* site mediates the antiferromagnetic interaction between the Cu^{2+} spins through Cu−O−Ti−O−Cu paths. Mn−O−Mn superexchange interaction does not seem to be responsible for the antiferromagnetism of $YMn_3Al_4O_{12}$ because one of the Mn−O bond lengths (2.69 Å) in the Mn−O−Mn paths is too long to mediate such interaction and because the Mn−O−Mn bond angle (101°) is far from the 180° expected to induce antiferromagnetic interaction according to the Kanamori−Goodenough rule. Instead, Mn−Mn direct exchange interaction appears to play a major role in the antiferromagnetism of $YMn_3Al_4O_{12}$ not unlike the major role for Cu−Cu direct exchange interaction in the ferromagnetism of $CaCu_3Sn_4O_{12}$. In $YMn_3Al_4O_{12}$ half-filled d_{z^2} and d_{xy} orbitals of the nearest neighboring Mn ions are directed toward each other (inset of Figure 6). Thus the overlap of those orbitals

can produce antiferromagnetic direct exchange interaction between the Mn spins.

Conclusions

$YMn_3Al_4O_{12}$ was synthesized at 9 GPa and 1173 K using a multianvil-type high-pressure apparatus. Bond valence sum calculations using the synchrotron X-ray powder diffraction data and the results of X-ray absorption spectroscopy measurement revealed that the oxidation state of each constituent cation was +3. Consequently, the compound has an ionic composition $Y^{3+}Mn^{3+}{}_3Al^{3+}{}_4O^{2-}{}_{12}$ with magnetic Mn^{3+} at the A' site and non-magnetic Al^{3+} at the B site. Magnetic measurements revealed that the A'-site Mn^{3+} ions are in a high-spin state and that they align antiferromagnetically at T_N = 34.3 K. Electronic structure calculations further revealed that the Al orbitals do not contribute to the magnetic interaction between the Mn^{3+} spins. The antiferromagnetic interaction in this material is attributed to the nearest Mn−Mn direct exchange interaction.

Acknowledgment. We thank M. Azuma for useful discussion. The synchrotron radiation experiments were performed at SPring-8 with the approval of the Japan Synchrotron Radiation Research Institute (Proposal Number: 2008B1222). This work was partly supported by Grants-in-Aid for Scientific Research (19GS0207, 18350097, and 17105002), by the Global COE Program "International Center for Integrated Research and Advanced Education in Materials Science" and by the Joint Project of Chemical Synthesis Core Research Institutions from the Ministry of Education, Culture, Sports, Science, and Technology, Japan.